Leveraging Multi-echo EPI to Enhance BOLD Sensitivity in Task-based Olfactory fMRI

Ludwig Sichen Zhao[*1,2], Clara U. Raithel[3,2], M. Dylan Tisdall[4], John A. Detre[2,4], and Jay A. Gottfried[*2,3]

[1]*Department of Bioengineering, School of Engineering and Applied Science, University of Pennsylvania, Philadelphia, PA, United States*
[2]*Department of Neurology, Perelman School of Medicine, University of Pennsylvania, Philadelphia, PA, United States*
[3]*Department of Psychology, School of Arts and Sciences, University of Pennsylvania, Philadelphia, PA, United States*
[4]*Department of Radiology, Perelman School of Medicine, University of Pennsylvania, Philadelphia, PA, United States*

* Corresponding Author: Ludwig Sichen Zhao (ludwigz@seas.upenn.edu), Jay A. Gottfried (jaygottf@pennmedicine.upenn.edu)

Abstract

Functional magnetic resonance imaging (fMRI) using blood-oxygenation-level-dependent (BOLD) contrast relies on gradient echo echo-planar imaging (GE-EPI) to quantify dynamic susceptibility changes associated with the hemodynamic response to neural activity. However, acquiring BOLD fMRI in human olfactory regions is particularly challenging due to their proximity to the sinuses where large susceptibility gradients induce magnetic field distortions. BOLD fMRI of the human olfactory system is further complicated by respiratory artifacts that are highly correlated with event onsets in olfactory tasks.

Multi-Echo EPI (ME-EPI) acquires gradient echo data at multiple echo times (TEs) during a single acquisition and can leverage signal evolution over the multiple echo times to enhance BOLD sensitivity and reduce artifactual signal contributions. In the current study, we developed a ME-EPI acquisition protocol for olfactory task-based fMRI and demonstrated significant improvement in BOLD signal sensitivity over conventional single-echo EPI (1E-EPI). The observed improvement arose from both an increase in BOLD signal changes through a T_2^*-weighted echo combination and a reduction in non-BOLD artifacts through the application of the Multi-Echo Independent Components Analysis (ME-ICA) denoising method. This study represents one of the first direct comparisons between 1E-EPI and ME-EPI in high-susceptibility regions and provides compelling evidence in favor of using ME-EPI for future task-based fMRI studies.

Keywords: multi-echo EPI, olfaction, ME-ICA, susceptibility artifacts, task-based fMRI

1 Introduction

Functional magnetic resonance imaging (fMRI) is one of the most common imaging techniques used to non-invasively study both localized neural activation and whole-brain functional connectivity in humans. Blood-oxygenation-level-dependent (BOLD) fMRI measures brain activity by detecting local magnetic susceptibility fluctuations caused by changes in deoxyhemoglobin concentration. Gradient echo echo-planar imaging (GE-EPI) is the dominant BOLD imaging strategy due to its high temporal signal-to-noise ratio and rapid acquisition capabilities (Budde et al., 2014). However, artifacts caused by the local inhomogeneous magnetic field surrounding high-susceptibility regions present a major technical challenge in utilizing GE-EPI to measure BOLD signals. Olfactory regions, including the orbitofrontal cortex (OFC), amygdala, piriform (olfactory) cortex, and entorhinal cortex are particularly affected by susceptibility-induced artifacts and signal drop-out due their location near the ethmoid sinuses (air-filled cavities in the bone surrounding the nose). These artifacts limit the applicability of GE-EPI-based BOLD fMRI in pursuit of understanding the human olfactory system (Catani et al., 2013). Moreover, respiratory artifacts, primarily caused by local field shifts during inhalation and exhalation that are highly correlated with event onsets in tasked-based olfactory-related fMRI, further compromise the sensitivity of olfactory fMRI (Glover & Law, 2001).

Several techniques have been proposed to overcome these challenges. Acquiring scans at a tilted angle allows for partial compensation of local susceptibility gradients (Deichmann et al., 2003; Weiskopf et al., 2006). Alternatively, employing pulse sequences other than GE-EPI, such as T_2-Prepared BOLD fMRI and balanced steady state free precession (bSSFP) (Parrish et al., 2008; Miao et al., 2021).

Recent work on multi-echo EPI (ME-EPI), which acquires multiple gradient echoes at each imaging timepoint, has shown potential to improve BOLD sensitivity and efficiency in resting-state fMRI (Gonzalez-Castillo et al., 2016; Lynch et al., 2020). In conventional single-echo EPI (1E-EPI), a single volume is acquired after each RF excitation at a specific echo time (TE), which determines both image signal intensity as well as BOLD contrast (Donahue et al., 2011; Gati et al., 1997; van der Zwaag et al., 2009). At a

shorter TE, the image is more proton-density weighted, has less BOLD contrast, and less severe signal dropout in regions with high local susceptibility gradients. Conversely, with a longer TE, the image becomes more T_2^*-weighted, has greater BOLD contrast, and more severe signal dropout. The BOLD contrast-to-noise ratio (CNR) is expected to vary with TE, peaking at the T_2^* of each voxel (Donahue et al., 2011; Fera et al., 2004; Gati et al., 1997; Graham et al., 1996; Triantafyllou et al., 2011; van der Zwaag et al., 2009). However, various brain regions exhibit distinct T_2^* values, resulting in varying optimal TEs, making it impossible to optimize TE across the whole brain in a single-echo acquisition.

Unlike 1E-EPI, ME-EPI acquires multiple images across a range of TEs after each RF excitation, resulting in enhanced functional contrast by combining the echo images with different weights (Poser et al., 2006; Posse et al., 1999). The commonly used T_2^*-weighted echo combination method assigns the heaviest weight to the echo that is presumed to have the greatest BOLD CNR, with weighting performed separately for each voxel. By applying a T_2^*-weighted echo combination with ME-EPI, BOLD signal can be maximized at the voxel level while maintaining the temporal resolution needed for fMRI. Moreover, by leveraging the expected exponential signal decay across TEs for true BOLD contrast, noise reduction techniques can be employed to reject artifactual signals and thereby improve the BOLD contrast-to-noise ratio (DuPre et al., 2021; Gonzalez-Castillo et al., 2016; Kundu et al., 2012a, 2013, 2017; Van et al., 2023).

In this study, we implemented and tested a ME-EPI acquisition protocol and analysis pipeline specifically designed for task-based olfactory-related paradigms by incorporating shorter TE values in an effort to improve sensitivity in ventral brain regions with high static susceptibility. Using this approach in comparison to a standard 1E-EPI acquisition, we demonstrate superior sensitivity to olfactory task activation resulting in a significant sample size reduction for detecting group task activation during a representative olfactory three-alternatives forced choice task (3AFC). Our findings suggest that ME-EPI holds great promise for human olfactory fMRI research.

2 Method

2.1 Subjects

29 subjects (13 women; aged 22 – 30 years, mean: 26, SD: 3.15) provided informed consent as approved by the University of Pennsylvania Institutional Review Board (#827217). One subject was excluded from the study due to excessive motion during fMRI scanning session, leaving us with a final sample of n = 28. All subjects reported being right-handed nonsmokers with no history of significant neurological/psychiatric disorder or olfactory dysfunction.

2.2 Odor Stimuli and Delivery

Stimuli consisted of two odorants: lemon oil extract (12.3% v/v, Sigma-Aldrich, MO, USA) and benzaldehyde (0.42% v/v, Sigma-Aldrich, MO, USA). Both odorants were diluted in mineral oil (Sigma Aldrich, MO, USA). Mineral oil alone was used as a control stimulus. The odor stimuli were delivered through a custom-built computer-controlled air-diluted 12-channel olfactometer with a flow rate of 4 L/min controlled using the PsychToolbox package (Brainard, 1997) and MATLAB (Version 2020b, The Mathworks Inc., Natick, MA, USA.)

2.3 Behavioral Testing Session

On Day 0, subjects participated in a behavioral testing session during which odor stimuli were presented outside the MRI environment. Participants were introduced to the odors and asked to label them as well as to rate the perceived odor intensity, via the general Labeled Magnitude Scale (gLMS) (Green et al., 1993, 1996). Valence (likeability) was also assessed via the Labeled Hedonic Scale (LHS) (L. V. Jones et al., 1955; Lim et al., 2009; Schutz & Cardello, 2001; Stone et al., 2020)], as well as familiarity [Visual Analog Scale (VAS) (Dourado et al., 2021; Flint et al., 2000)]. Ratings were analyzed in MATLAB (Version 2020b, The Mathworks Inc., Natick, MA, USA), using three one-way ANOVAs to evaluate whether there were any differences among stimuli.

2.4 fMRI Scanning Session

2-5 days after the behavioral testing session, the same participants took part in an fMRI scanning session, completing six runs, each of which contained 24 trials. On each trial, participants sniffed one of the three possible odorants (lemon oil extract, benzaldehyde, or mineral oil) and were asked to identify the odor using a three-alternative forced choice task with the labels they provided earlier during the behavioral testing session. Following the 3AFC task, they were also asked to rate the intensity of the odor. Each odor was presented eight times per run in a random order. The experimental paradigm as well as the sequence of events within a given trial is shown in Figure 1b.

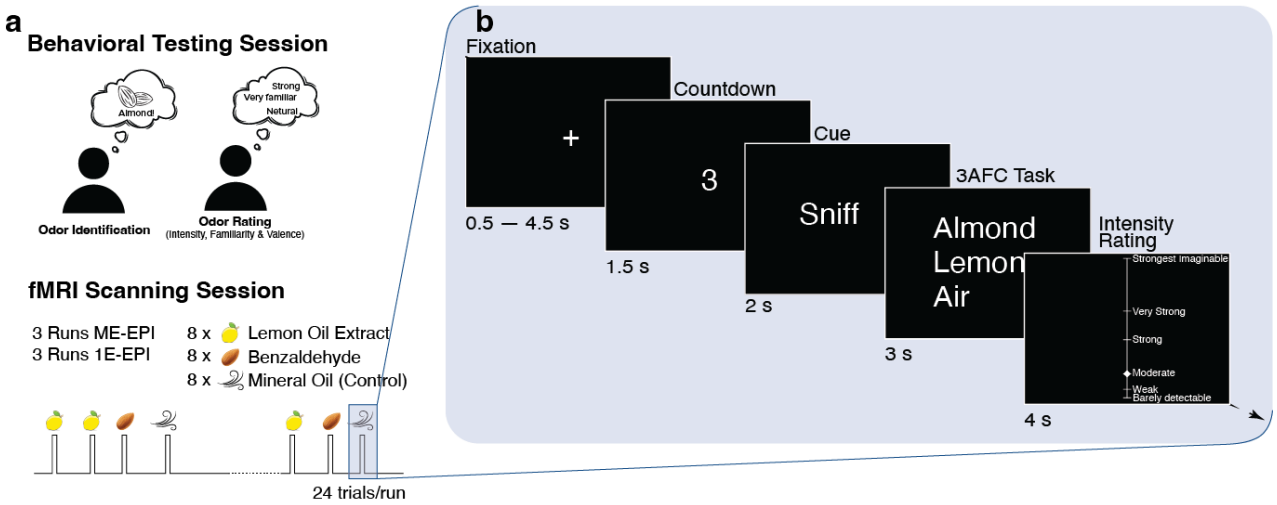

Figure 1. fMRI Experimental Paradigm. a) The experiment was conducted over the course of two *sessions*. On Day 0, the subjects participated in a series of behavioral tests where they were required to identify odors and rate their intensity, valence, and familiarity. Subsequently, an fMRI scanning session was scheduled for the subjects, taking place two to five days after their initial visit. This scanning session consisted of three runs of ME-EPI and three runs of 1E-EPI acquisition. Each run comprised 24 trials, with an equal distribution of three odor stimuli: lemon oil extract, benzaldehyde, and mineral oil. b) Timeline for a single trial. A trial started with a fixation cross presented for 0.5 – 4.5 s, followed by a 1.5 s countdown. A cue to sniff was then displayed and the odor was delivered for 2 s. Participants were then asked to identify the odor and rate its intensity.

2.5 Structural and Functional MRI Data Acquisition

All magnetic resonance images were acquired using a 3 T scanner (MAGNETOM Prisma, Siemens Healthineers, Germany) using the vendor's 64-channel head and neck

138 coil. T_1-weighted structural images were acquired using ME-MPRAGE (TE =
139 1.69/3.55/5.41/7.27 ms, TR = 2530 ms, TI = 1100 ms, FA = 8°, 1 mm isotropic).

140 1E-EPI and ME-EPI fMRI data were acquired using the sequence parameters outlined
141 in Table 1. For both protocols, repetition time (TR), field of view (FOV), number of
142 slices, resolution, flip angle (FA), echo spacing, and multiband factors are identical. To
143 optimize the BOLD signals in OFC regions, the field of view was tilted approximately 25°
144 to the anterior commissure-posterior commissure line (rostral > caudal) (Deichmann et
145 al., 2003). The two sequence types were administered in an interleaved fashion in each
146 participant, with the order being counterbalanced across participants. Of note, for 1E-
147 EPI the echo time was set at 22 ms, which is approximately the same as the second
148 echo time out of five echoes in the ME-EPI sequence (see Table 1). This TE aims to
149 balance signal dropout and BOLD sensitivity for olfactory-related regions and is
150 consistent with other olfactory-related fMRI studies (Bao et al., 2019; de Groot et al.,
151 2021; Raithel et al., 2023; Shanahan et al., 2021; Zhou et al., 2019).

	1E- EPI	**ME-EPI**
TR (ms)	2041	2041
TE (ms)	22	10.60/22.92/35.24/ 47.56/59.88
FOV (mm x mm)	216 x 216	216 x 216
Slices	48	48
Resolution (mm x mm x mm)	2.4 x 2.4 x 2.4	2.4 x 2.4 x 2.4
FA (degree)	78	78
Echo Spacing (ms)	0.49	0.49
Acceleration	Multiband 2x	Multiband 2x GRAPPA 3D, 3x

152 *Table 1. fMRI Sequence Parameters.* TR: Repetition time. TE: Echo time. FOV: Field of view. FA: Flip
153 angle. 1E-EPI: single-echo EPI. ME-EPI: multi-echo EPI.

2.6 fMRI Data Preprocessing

fMRI and structural MRI data were preprocessed in each subject's native space using fMRIPrep 21.0.0 based on Nipype 1.6.1 (Esteban et al., 2019; Gorgolewski et al., 2011). All images were then registered to ICBM 152 Nonlinear Asymmetrical template version 2009c (MNI-ICBM2009c) before further processing (Fonov et al., 2009, 2011).

2.7 ME-EPI T_2^* Estimation, Echo Combination, and Multi-Echo Independent Components Analysis (ME-ICA)

Multi-echo EPI produces separate images for each echo time at each timepoint in the functional imaging run. At each timepoint, these images for the multiple echo times were combined using the T_2^*-weighted combination method (ME-WC) (Posse et al., 1999). For each voxel, T_2^* was estimated by fitting the Eq. (1) using signals from all five echoes.

$$S = S_0 e^{-TE/T_2^*} \tag{1}$$

The images from the five echoes are then combined voxel-wise using a weighted average and the weights for each echo (W_{TE}) are calculated using Eq. (2) based on estimated T_2^*.

$$W_{TE} = \frac{TE \cdot exp(-TE/T_2^*)}{\sum_{n=1}^{5} TE_n \cdot exp(-TE_n/T_2^*)} \tag{2}$$

Independent components analysis (ICA) is a common strategy to decompose fMRI signals into distinct independent components, allowing the isolation of BOLD-related neuronal components from sources of noise (Beckmann, 2012; Caballero-Gaudes & Reynolds, 2017; Mckeown et al., 1998; McKeown et al., 2003). However, a persistent challenge lies in the manual classification of these independent components, which is labor-intensive and can yield inconsistent results (Kelly et al., 2010). In an attempt to tackle this problem, ME-ICA classifies each component as either a non-BOLD artifact, such as respiratory artifact, or a BOLD-like signal based on their signal characteristics across different echo times (Kundu et al., 2012b, 2013). Here, we specifically employed

178 the TE-dependency analysis pipeline (Tedana 0.0.12) (DuPre et al., 2021) to
179 preprocess multi-echo EPI data before registering them to the MNI template.

180 *2.8 Physiological Data Analysis*

181 The respiratory trace was recorded with a respiratory transducer using a pressure
182 sensor (BIOPAC System, CA, USA) affixed around the subject's chest, and then
183 preprocessed before being added as a nuisance regressor: the trace was smoothed
184 using a 250 ms moving window, high-pass filtered at 0.05 Hz, detrended, and
185 standardized. The preprocessed trace was also downsampled to 1/2.4 Hz to be
186 included as a nuisance regressor. Two additional nuisance regressors were introduced:
187 the trial-by-trial sniff volume was defined as the amplitude difference between inhalation
188 and exhalation, and the sniff duration was defined as the time difference between
189 inhalation and exhalation.

190 *2.9 Statistical Analysis*

191 All fMRI data were analyzed in SPM12 using a general linear model to estimate the
192 main effects of the odor stimulation. Each experimental condition (control, lemon oil,
193 and benzaldehyde) was modeled using an independent regressor for each run. This
194 results in a 2 (multi-echo and single-echo) by 3 (control, lemon oil, and benzaldehyde)
195 factorial design. The model included the following nuisance regressors: trial-by-trial sniff
196 volume and sniff duration, both convolved with the hemodynamic response function
197 (HRF), as well as the down-sampled breathing trace and 24 movement parameters (six
198 movement parameters derived from spatial realignment, their squares, derivatives, and
199 squares of derivatives). In all GLMs, data were high-pass filtered at 1/128 Hz; the
200 temporal autocorrelation was estimated and removed as an autoregressive AR(1)
201 process globally (Friston et al., 2002).

202 Contrasts of interest were defined as [Odor > Control], [Lemon > Control] and
203 [Benzaldehyde > Control]. Whole brain analysis was performed to validate that odor-
204 evoked activations were present in the data acquired through both protocols (1E-EPI
205 and ME-EPI). Small volume corrections (SVC) and ROI analysis were separately
206 performed on OFC, amygdala, piriform cortex and entorhinal cortex, as suggested by

207 previous studies highlighting the involvement of these regions in human olfactory
208 processing (Anderson et al., 2003). Amygdala and piriform cortex were defined
209 anatomically using a human brain atlas (Mai et al., 2016). Delineation of OFC and
210 entorhinal cortex were based on the MNI-ICBM2009c atlas (Manera et al., 2020).

211 *2.10 Post-hoc Power Analysis*

212 We used our ROI analysis results to estimate the sample sizes required to detect
213 significant olfactory-related group fMRI activation in subsequent studies. A priori power
214 analyses were performed with $\alpha = 0.05$ and $\beta = 0.80$ using G*Power (Faul et al., 2009)
215 for both ME-EPI and 1E-EPI data in the same ROIs described in the previous section.

216 3 Results

217 *3.1 Echo-combined Images Reduce Signal Dropout*

218 We first examined the estimated T_2^* values for each olfactory-related region. As
219 expected, signal dropouts are reduced in shorter echo times (Figure 2a, TE_1 and TE_2),
220 while T_2^*-weighted contrast is developed in later echo times (Figure 2a, TE_3 – TE_5). In
221 particular, the medial and lateral OFC along with the entorhinal cortex, exhibited notably
222 shorter T_2^* values due to susceptibility artifacts (Figure 2a & 2b), and in turn the echo-
223 combined image more heavily weights the shorter echoes (Figure 2c). Using these
224 weights, the combined image (Figure 2a, WC) effectively mitigated signal dropout while
225 retaining notable T_2^*-weighted contrast.

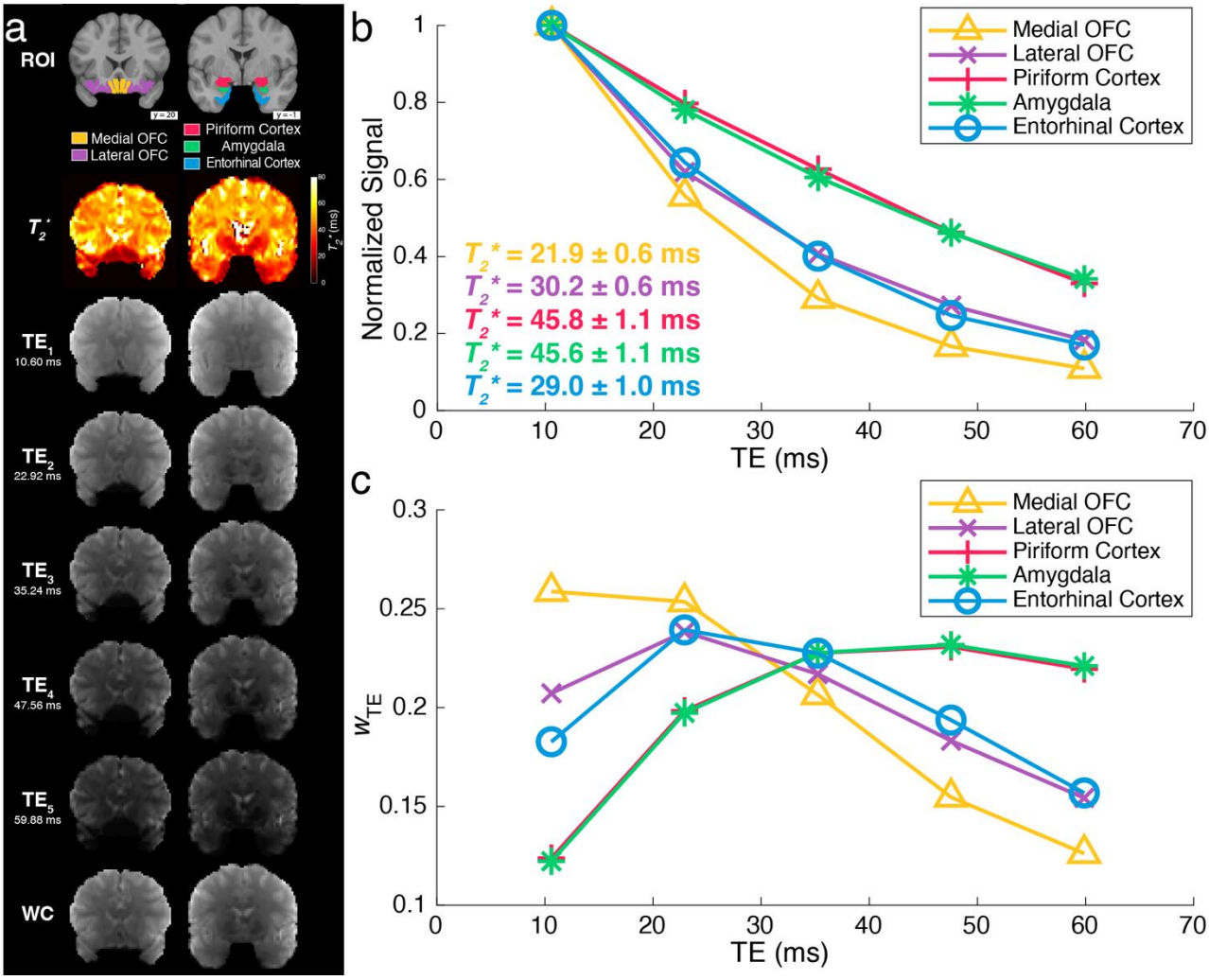

Figure 2. Multi-echo fMRI Reduces Signal Dropout and Improves BOLD Contrast through T_2^*-Weighted Combination in a Single Subject. A) Two representative coronal slices containing the ROIs of interest are shown with a variety of contrasts: ROIs overlayed on the T_1-weighted image (ROI); estimated T_2^* maps; all five individual echo images (TE_1 – TE_5) from the ME-EPI acquisition; and the T_2^*-weighted combined images (WC). b) Plot of signal vs echo time for each anatomical ROI. c) Within-ROI mean of the voxel-wise weights used to compute the T_2^*-weighted combined images.

3.2 BOLD Activation in Diverse Olfactory Brain Regions During Odor Stimulation

We next investigated the regions that were significantly activated when the odors were delivered under ME-EPI acquisition with the ME-ICA denoising method [Odor > Control] (Figure 3a) (DuPre et al., 2021). Consistent with previous literature, we observed significant activation in the piriform cortex, amygdala, entorhinal cortex, insula, and OFC bilaterally ($p < 0.001$, uncorrected) (Anderson et al., 2003; Dikecligil & Gottfried, 2024;

239 Gottfried et al., 2003; Howard & Gottfried, 2014; Patin & Pause, 2015; Plailly et al.,
240 2008). We next examined the BOLD effects of individual odor stimulus, namely
241 [Benzaldehyde > Control] and [Lemon > Control]. Despite statistical testing indicating no
242 significant differences in perceived intensity (p = 0.38), valence (p = 0.45), and
243 familiarity (p = 0.11) between benzaldehyde and lemon oil, our analysis revealed that
244 the main effect [Odor > Control] was driven mainly by the contrast [Lemon > Control]. In
245 comparison, the contrast [Benzaldehyde > Control] produced significant levels of
246 activation only in the bilateral insular region (Figure 3a). The difference in BOLD
247 response to these stimuli was not anticipated though not wholly unprecedented, as
248 previous research has demonstrated that different odors can elicit distinct responses
249 within olfactory brain regions even in the absence of differences in low-level stimulus
250 features (Fournel et al., 2016; Howard & Gottfried, 2014; Savic, 2002; Savic et al.,
251 2002). In the single-echo fMRI, a similar trend is observed, with more active regions
252 being detected with lemon oil (p < 0.05, uncorrected, Figure S1). Accordingly, to
253 compare and observe the differences between acquisition methods within olfactory
254 regions, we will focus on the activation under lemon oil condition [Lemon > Control] for
255 our further analyses.

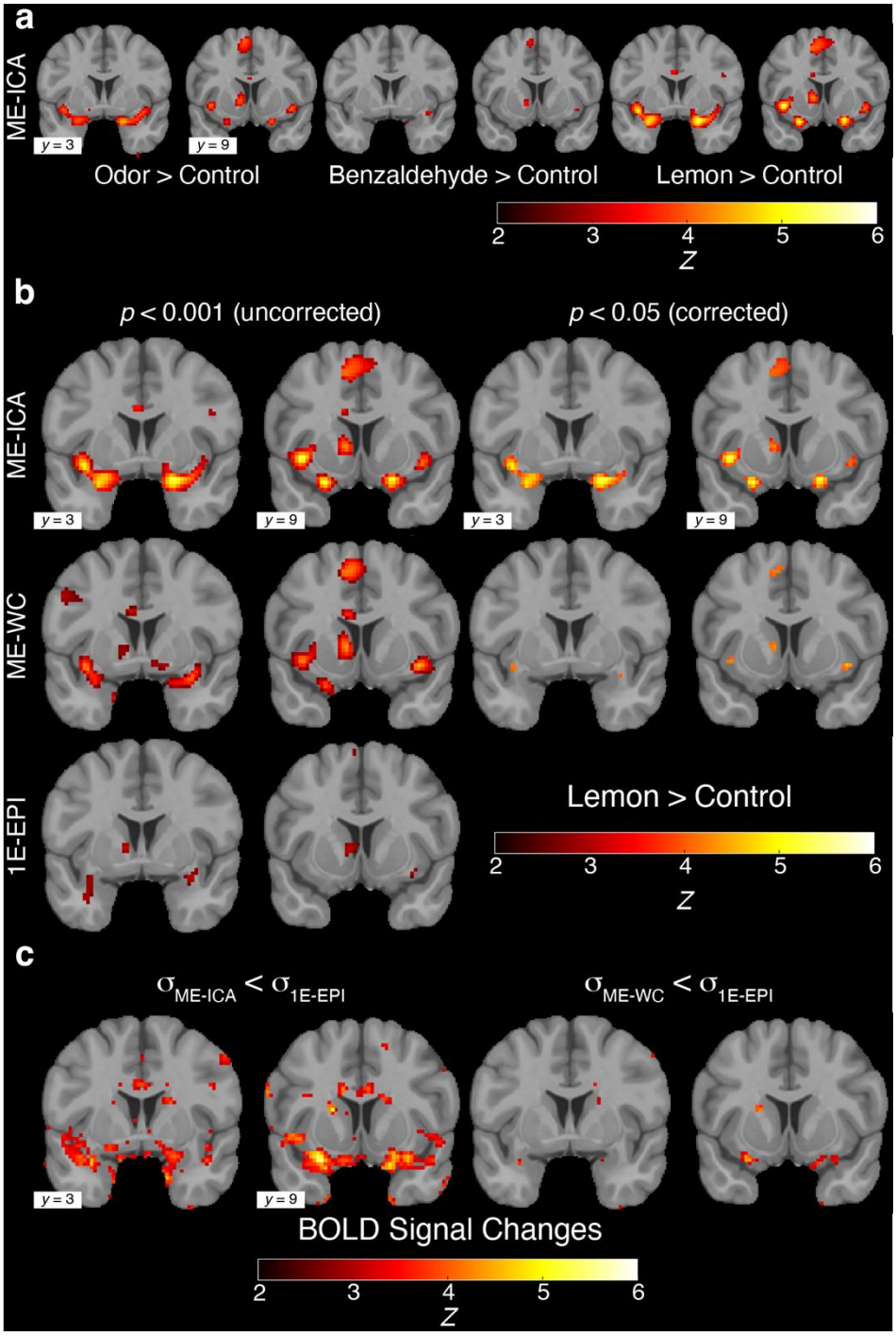

Figure 3. Activation Maps from Olfactory-related Task for Both 1E-EPI and ME-EPI. a) Two representative coronal slices of activation maps for all three contrasts ([Odor > Control], [Benzaldehyde > Control], [Lemon > Control]) using ME-EPI acquisition with ME-ICA denoising methods ($p < 0.05$, FDR corrected). b) Activation maps for [Lemon > Control] contrast for ME-EPI acquisition with ME-ICA denoising methods (ME-ICA), and without ME-ICA denoising methods (ME-WC) as well as single-echo fMRI acquisition (1E-EPI). The left two columns show the maps without multiple comparison correction ($p < 0.001$) while the

right two columns show the maps corrected for multiple comparison ($p < 0.05$, FDR corrected). No activation survived correction for multiple comparisons for 1E-EPI (not shown). c) *Z*-score statistical maps yielded from Levene's test to examine whether BOLD signal variance was lower in ME-WC [$\sigma_{ME\text{-}WC} < \sigma_{1E\text{-}EPI}$] and ME-EPI [$\sigma_{ME\text{-}ICA} < \sigma_{1E\text{-}EPI}$] compared to 1E-EPI ($p < 0.05$, FDR corrected).

3.3 ME-EPI Improves fMRI Signal Sensitivity by Both Increasing BOLD Signal Changes and Reducing non-BOLD Artifacts

Having validated that our ME-EPI acquisition protocol is suitable to capture odor-evoked BOLD responses, we next compared BOLD activation among different acquisition methods (1E-EPI vs. ME-EPI) and analysis pipelines (ME-WC vs. ME-ICA). A whole-brain analysis using either whole-brain multiple comparisons correction (FDR) (Benjamini & Hochberg, 1995; Benjamini & Yekutieli, 2001; Yekutieli & Benjamini, 1999) or small volume correction (SVC) did not yield any supra-threshold voxels for 1E-EPI. However, the same whole-brain analysis using the T_2^*-weighted combined ME-EPI (ME-WC) highlighted activation in all ROIs (piriform cortex, amygdala, OFC, and entorhinal cortex) (Figure 3b). Moreover, by using ME-ICA denoising methods (DuPre et al., 2021), we observed a further increase in both the number of activation voxels and peak *Z* values in all ROIs (Table 2).

	Piriform Cortex		**Amygdala**		**Entorhinal Cortex**		**OFC**	
	# Voxel	**Peak *Z***	**# Voxel**	**Peak *Z***	**# Voxel**	**Peak *Z***	**# Voxel**	**Peak *Z***
ME-ICA	167	5.44	9	4.31	12	4.14	32	5.44
ME-WC	5	4.04	2	3.98	1	3.74	10	4.44
1E-EPI	0	N/A	0	N/A	0	N/A	0	N/A

Table 2. Number of Voxels and Peak Z-score Activated by Lemon Oil for each ROI ($p < 0.05$, SVC).

We next examined potential reasons for the observed differences. Specifically, we hypothesized the improvement of the BOLD sensitivity in the case of the ME-EPI data was due to more pronounced BOLD signal changes, as we performed a locally weighted combination of all echoes for each individual voxel instead of using one single TE across the brain. BOLD signal changes could be calculated by contrast estimates from the general linear model (GLM). Therefore, we performed a paired *t*-test on contrast estimates [Lemon > Control] between 1E- and ME-EPI with ME-ICA [ME-ICA > 1E-EPI] among all ROIs. Only piriform cortex ($p = 0.023$) and lateral OFC ($p = 0.006$)

289 showed greater estimates for the contrast [Lemon > Control] for ME-ICA compared to
290 1E-EPI.

291 An alternative explanation for the observed differences between acquisition protocols,
292 that is, the increased BOLD sensitivity for ME-EPI versus 1E-EPI, may lie in the
293 reduction of the background noise due to non-BOLD signals. To test the hypothesis that
294 ME-EPI signal changes have a lower variance, we performed a Levene's test (Levene,
295 1960). This test is commonly employed to assess whether two or more groups have
296 equal variances in a dataset (Chiarello et al., 2009; Farinha et al., 2022; Im et al., 2010;
297 T. B. Jones et al., 2010; Swarup et al., 2013). Using a whole-brain analysis we first
298 generated a mask using the voxels activated by the [Lemon > Control] contrast and $p <$
299 0.001 (uncorrected) through the ME-ICA acquisition and process. Within this mask, we
300 find that 2.98% of these masked voxels reached the significance threshold ($p < 0.05$,
301 FDR corrected) for Levene's test comparing ME-WC and 1E-EPI. This result aligns with
302 prior research indicating that ME-EPI, even without the application of ME-ICA, has the
303 potential to decrease non-BOLD noise in resting-state analysis (Kundu et al., 2017;
304 Lynch et al., 2020; Posse et al., 1999). Subsequently, we aimed to assess whether
305 using ME-ICA can reduce noise above and beyond ME-WC. Indeed, the number of
306 significant voxels further increased to 23.1% of masked voxels when comparing ME-ICA
307 and 1E-EPI (Figure 3c). Taken together, our data suggest that our observed increase in
308 BOLD detection is not only due to increased sensitivity BOLD signals, but also the
309 reduction of non-BOLD artifacts.

310 *3.4 ME-EPI Improves Statistical Power and Reduces Sample Sizes*

311 So far, we have established that ME-EPI improved BOLD signal sensitivity by both
312 enhancing BOLD signal and reducing non-BOLD artifacts. An outstanding question is to
313 what degree BOLD sensitivity is improved when using our suggested method in the
314 context of task-based olfactory fMRI. To quantify the change in BOLD sensitivity, we
315 examined the contrast [Lemon > Control] in the brain regions central to olfaction,
316 namely the piriform cortex, amygdala, lateral and medial OFC, and entorhinal cortex for
317 both acquisition methods separately and then compared the statistical outcomes.
318 Whereas activation in medial OFC did not reach statistical significance using data

resulting from either acquisition method, all remaining regions show much lower *p*-values for ME-ICA compared to 1E-EPI (Table 3). Furthermore, to determine the minimum sample size required to observe significance in each region, post-hoc power analyses were carried out (α = 0.05 and β = 0.80) to estimate the effect of each acquisition method on the sample sizes needed to detect effects in similar olfactory task fMRI studies. ME-ICA led to a substantial reduction in the sample size, ranging from by half to one-fourth, compared to 1E-EPI, depending on the specific regions (Figure 4).

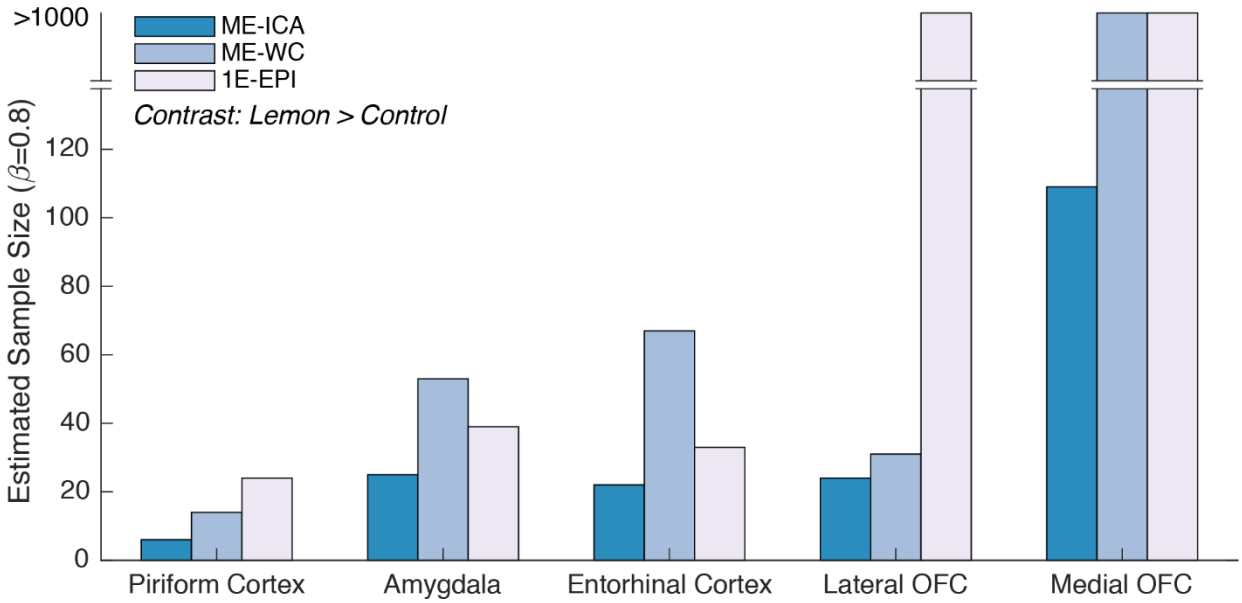

Figure 4. Estimated Sample Size for ROI Analyses Based on Post-hoc Power Analyses (α = 0.05 and β = 0.80) in all Olfactory-related ROIs under Contrast [Lemon > Control] for Single-echo fMRI (1E-EPI), ME-EPI BOLD Acquisition with ME-ICA Denoising Methods (ME-ICA), and without ME-ICA Denoising Methods (ME-WC).

	Piriform Cortex	**Amygdala**	**Entorhinal Cortex**	**Lateral OFC**	**Medial OFC**
ME-ICA	< 0.0001***	0.007***	0.005**	0.006**	0.884
ME-WC	0.0006***	0.044*	0.065	0.0138*	0.612
1E-EPI	0.007**	0.024*	0.0157*	0.549	0.669

p < 0.001 *** *p* < 0.01 ** *p* < 0.05 *

Table 3. Statistical Significance of ROI Analyses for Each Olfactory-related ROI under the Contrast [Lemon > Control] for 1E-EPI, ME-WC and ME-ICA.

4 Discussion

Susceptibility artifacts pose a significant challenge when using GE-EPI for fMRI studies. The primary olfactory cortex not only suffers from some of the most severe static susceptibility artifacts within the human brain but is also affected by respiration-related artifacts. Here, we have developed and validated a ME-EPI protocol and analysis pipeline specifically tailored for olfactory task-based fMRI. In the context of a basic olfactory 3AFC task, we found that ME-EPI, alongside ME-ICA denoising, systemically improves BOLD sensitivity and reduces the required sample sizes needed to infer a significant effect at a group level compared to conventional 1E-EPI. This is achieved by both increasing BOLD signal sensitivity and reducing the contributions of non-BOLD signal changes using the additional denoising features ME-EPI provided.

The echo times used for ME-BOLD provided a range of contrasts across different TEs for each ROI of interest (Figure 2a). When evaluating the T_2^*-derived weights calculated for the echo-combined image, we confirmed that high-susceptibility regions with short T_2^* values, namely, lateral and medial OFC, and entorhinal cortex, had higher weights assigned to the first two echoes. In contrast, the remaining ROIs had higher weights assigned to the remaining (and later) three echoes. As a result, the T_2^*-weighted combined (WC) images were able to produce more uniform T_2^*-weighted contrast across the whole brain (Figure 2a, WC).

When investigating the region activated by odor onset using ME-ICA, we detected activation in all major primary olfactory cortex regions (piriform cortex, amygdala, entorhinal cortex, and OFC bilaterally) in addition to the insular region (Figure 3a). These findings are consistent with previous literature (Anderson et al., 2003; Dikecligil & Gottfried, 2024; Gottfried et al., 2003; Howard & Gottfried, 2014; Patin & Pause, 2015; Plailly et al., 2008). Further analysis revealed that the activation was primarily driven by the lemon extract stimulus in comparison to benzaldehyde. Previous studies have demonstrated that different odor stimuli can activate distinct primary olfactory regions to different degrees (Fournel et al., 2016; Howard & Gottfried, 2014; Savic, 2002; Savic et al., 2002). In this study we found that that benzaldehyde activates the olfactory system

364 to a lesser extent than lemon oil, such that the observed activation did not reach
365 significance after correcting for multiple comparisons in the whole brain analysis.

366 When comparing the results of 1E-EPI and ME-EPI, we observed significantly increased
367 sensitivity in both whole brain analysis and ROI analysis, which are two commonly used
368 univariate fMRI analysis methods. In the case of whole brain analysis (Figure 3b), we
369 found that ME-EPI exhibited higher peak *Z* values and a greater number of activated
370 voxels compared to 1E-EPI, as shown in Table 2. It is worth noting that even without
371 using the ME-ICA denoising method, ME-EPI still outperformed 1E-EPI by performing a
372 T_2^*-weighted combination of data from all echoes. This improvement was expected, as
373 the weighting of data from each echo time was designed to enhance the sensitivity to
374 BOLD contrast (Posse et al., 1999).

375 For ROI analysis and sequential power analysis, which were used to estimate minimal
376 sample sizes, ME-EPI with the ICA denoising method demonstrated superiority over 1E-
377 EPI, as shown in Table 3 and Figure 4. We attribute these improvements to two factors:
378 the increase of BOLD signal intensity through T_2^*-weighted echo combination and the
379 reduction of noise by leveraging signal evaluation across the echo times. To support
380 these hypotheses, we conducted a series of statistical tests (Figure 3c) to show the
381 mean signals are significantly higher and the variance is significantly lower in ME-ICA
382 acquisition compared to 1E-EPI.

383 The current analysis pipeline employs a specific method of combining multiple echo
384 image series into a single image series: T_2^*-weighted combination, also known as
385 "optimal combination", is used in most ME-EPI studies as it is designed to maximize
386 BOLD-contrast sensitivity (Baracchini et al., 2021; Gonzalez-Castillo et al., 2016; Kundu
387 et al., 2017; Lynch et al., 2020; Roth et al., 2020). However, an interesting finding
388 emerged when we processed the ME-EPI data separately and treated each individual
389 echo series as a 1E-EPI dataset. Surprisingly, no supra-threshold activation was
390 detected at the first echo ($p < 0.05$, uncorrected), while the majority of activations were
391 observed at the second and third echoes ($p < 0.05$, uncorrected). When examining the
392 *Z* values for the ROI analyses across all 5 individual echoes, we also observe a similar
393 trend (Table S1). However, regions with short T_2^* (such as the lateral and medial OFC

394 and entorhinal cortex in this study) predominantly assigned higher weights to the first
395 two echoes.

396 In addition to the incongruence between apparent BOLD signal in the earliest echo and
397 the weight assigned to it, T_2^* values near the ethmoid sinuses fluctuate during inhalation
398 and exhalation due to local B_0 field shifts (Barry & Menon, 2005; Raj et al., 2000, 2001;
399 Van de Moortele et al., 2002). In olfactory studies, this causes significant task-related
400 artifacts. The T_2^*-weighted combination method used in our current analyses employed
401 fixed weighting throughout one scan and does not account for this dynamic T_2^*
402 fluctuation; the use of dynamically adjusted weights might also improve BOLD
403 sensitivity. Further work is required to determine if more information could be used to
404 choose optimal echo weightings that might further increase BOLD-sensitivity (*e.g.*, by
405 reducing the weights on the first echo, even in the short- T_2^* voxels). These findings
406 may, in part, elucidate the observed effects in Table 2 and Figure 4, wherein the
407 estimated sample sizes are higher, and the statistical significances are lower for ROI
408 analyses in certain regions for ME-WC compared to 1E-EPI.

409 There have also been recent advances in denoising methods that leverage phase
410 information, such as Noise Reduction with Distribution Corrected (NORDIC) PCA
411 (Dowdle et al., 2023; Moeller et al., 2021; Vizioli et al., 2021). These methods have
412 demonstrated the ability to further enhance BOLD sensitivity in resting-state fMRI.
413 However, our study did not acquire phase data, which prevented us from testing these
414 advanced denoising methods in our data.

415 In this study, we utilized a limited set of two odor stimuli, along with a control stimulus.
416 Although this approach was adequate to compare the ME-EPI and 1E-EPI acquisition
417 methods, future studies will aim to incorporate a wider range of odor stimuli. By
418 including multiple odor stimuli, we can expand our analysis to encompass multivariate
419 analysis, such as Multivariate Pattern Analysis (MVPA), which has been commonly
420 utilized in other olfaction task-based fMRI studies (Donoshita et al., 2021; Howard et al.,
421 2009; Howard & Gottfried, 2014; Perszyk et al., 2023), though we expect also to see an
422 improvement in multivariate analysis using ME-ICA.

In conclusion, our study demonstrated the utility of a ME-EPI protocol combined with a pre-configured analysis pipeline for fMRI in olfactory cortex. This approach enhanced sensitivity to task-dependent BOLD contrast changes in olfactory regions, and post-hoc power analyses indicate that group effects can be detected with a reduced sample size compared to standard 1E-EPI. Although our protocol and pipeline were specifically designed for task-based fMRI in the presence of large static susceptibility, a longstanding challenge in the field of fMRI, they showcase the superior denoising capabilities of ME-EPI for task-based fMRI more generally. These findings strongly support the adoption of ME-EPI over 1E-EPI for future task-based fMRI studies.

Data and Code Availability

The unthresholded *Z*-maps showing the whole-brain results for univariate analyses were made available on Neurovault (https://neurovault.org/collections/KGZMOMWR/).

Author Contributions

Ludwig Sichen Zhao: Conceptualization, Methodology, Software, Formal Analysis, Investigation, Data Curation, Visualization, Writing – Original Draft, Project administration. **Clara U. Raithel**: Conceptualization, Methodology, Investigation, Writing – Review & Editing. **M. Dylan Tisdall**: Conceptualization, Methodology, Writing – Review & Editing, Supervision, Resources. **John A. Detre**: Conceptualization, Methodology, Writing – Review & Editing, Supervision, Resources. **Jay A. Gottfried**: Conceptualization, Methodology, Writing – Review & Editing, Supervision, Resources, Funding acquisition

Funding

This work was supported by the National Institutes of Health award R01DC019405 [awarded to JAG].

Declaration of Competing Interests

The authors have declared that no competing interests exist.

Supplementary Materials

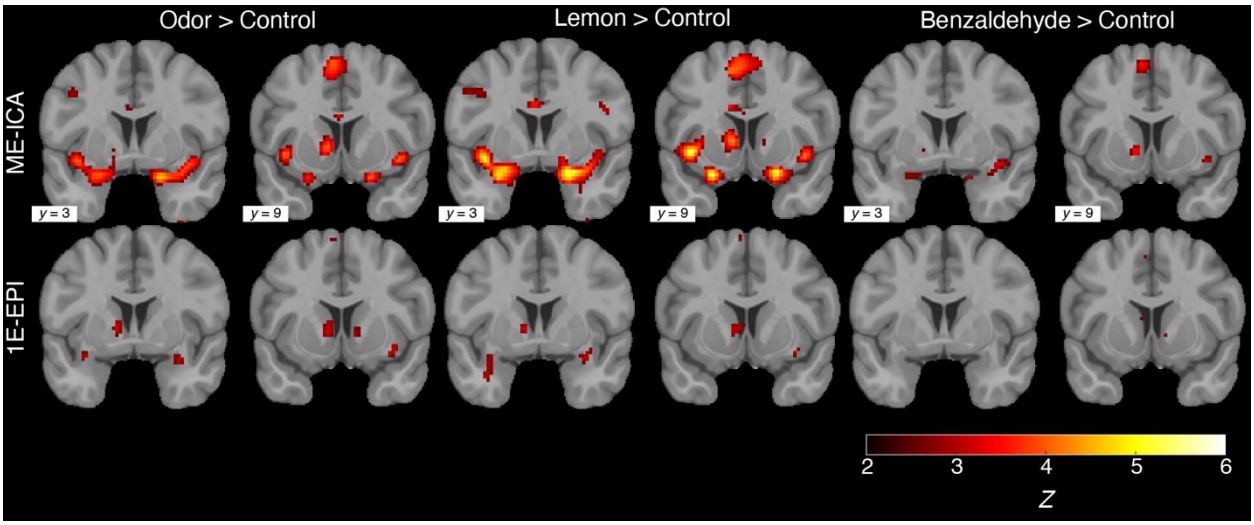

Figure S1. Comparison of Activation Maps Among Different Contrasts for Olfactory-Related Tasks in Both 1E-EPI and ME-EPI. Two representative coronal slices of activation maps for all three contrasts ([Odor > Control], [Benzaldehyde > Control], [Lemon > Control]) using ME-EPI acquisition with ME-ICA denoising methods (ME-ICA) and using single-echo fMRI (1E-EPI) acquisition ($p < 0.001$, uncorrected).

	Piriform Cortex	**Amygdala**	**Entorhinal Cortex**	**Orbitofrontal Cortex**
TE_1 (10.60 ms)	1.945	1.010	0.756	1.205
TE_2 (22.92 ms)	2.383	1.957	2.183	1.605
TE_3 (35.24 ms)	3.457	1.583	1.789	1.724
TE_4 (47.56 ms)	3.819	1.355	0.973	1.835
TE_5 (59.98 ms)	3.693	2.604	1.265	1.705

Table S1. Z Scores of ROI Analyses for Each Olfactory-related ROI under the Contrast [Lemon > Control] When Analyzing 5 Individual Echoes from ME-ICA Separately.

References

Anderson, A. K., Christoff, K., Stappen, I., Panitz, D., Ghahremani, D. G., Glover, G., Gabrieli, J. D. E., & Sobel, N. (2003). Dissociated neural representations of intensity and valence in human olfaction. *Nature Neuroscience*, *6* (2), Article 2. https://doi.org/10.1038/nn1001

Bao, X., Gjorgieva, E., Shanahan, L. K., Howard, J. D., Kahnt, T., & Gottfried, J. A. (2019). Grid-like Neural Representations Support Olfactory Navigation of a Two-Dimensional Odor Space. *Neuron*, *102* (5), 1066-1075.e5. https://doi.org/10.1016/j.neuron.2019.03.034

Baracchini, G., Mišić, B., Setton, R., Mwilambwe-Tshilobo, L., Girn, M., Nomi, J. S., Uddin, L. Q., Turner, G. R., & Spreng, R. N. (2021). Inter-regional BOLD signal variability is an organizational feature of functional brain networks. *NeuroImage*, *237*, 118149. https://doi.org/10.1016/j.neuroimage.2021.118149

Barry, R. L., & Menon, R. S. (2005). Modeling and suppression of respiration-related physiological noise in echo-planar functional magnetic resonance imaging using global and one-dimensional navigator echo correction. *Magnetic Resonance in Medicine*, *54* (2), 411–418. https://doi.org/10.1002/mrm.20591

Beckmann, C. F. (2012). Modelling with independent components. *NeuroImage*, *62* (2), 891–901. https://doi.org/10.1016/j.neuroimage.2012.02.020

Benjamini, Y., & Hochberg, Y. (1995). Controlling the False Discovery Rate: A Practical and Powerful Approach to Multiple Testing. *Journal of the Royal Statistical Society: Series B (Methodological)*, *57* (1), 289–300. https://doi.org/10.1111/j.2517-6161.1995.tb02031.x

Benjamini, Y., & Yekutieli, D. (2001). The control of the false discovery rate in multiple testing under dependency. *The Annals of Statistics*, *29* (4), 1165–1188. https://doi.org/10.1214/aos/1013699998

Brainard, D. H. (1997). The Psychophysics Toolbox. *Spatial Vision*, *10* (4), 433–436. https://doi.org/10.1163/156856897X00357

Budde, J., Shajan, G., Zaitsev, M., Scheffler, K., & Pohmann, R. (2014). Functional MRI in human subjects with gradient-echo and spin-echo EPI at 9.4 T. *Magnetic Resonance in Medicine*, *71* (1), 209–218. https://doi.org/10.1002/mrm.24656

Caballero-Gaudes, C., & Reynolds, R. C. (2017). Methods for cleaning the BOLD fMRI signal. *NeuroImage*, *154*, 128–149. https://doi.org/10.1016/j.neuroimage.2016.12.018

Catani, M., Dell'Acqua, F., & Thiebaut de Schotten, M. (2013). A revised limbic system model for memory, emotion and behaviour. *Neuroscience & Biobehavioral Reviews*, *37* (8), 1724–1737. https://doi.org/10.1016/j.neubiorev.2013.07.001

Chiarello, C., Welcome, S. E., Halderman, L. K., Towler, S., Julagay, J., Otto, R., & Leonard, C. M. (2009). A large-scale investigation of lateralization in cortical anatomy and word reading: Are there sex differences? *Neuropsychology*, *23* (2), 210–222. https://doi.org/10.1037/a0014265

de Groot, J. H. B., Kirk, P. A., & Gottfried, J. A. (2021). Titrating the Smell of Fear: Initial Evidence for Dose-Invariant Behavioral, Physiological, and Neural Responses. *Psychological Science*, *32* (4), 558–572. https://doi.org/10.1177/0956797620970548

Deichmann, R., Gottfried, J. A., Hutton, C., & Turner, R. (2003). Optimized EPI for fMRI studies of the orbitofrontal cortex. *NeuroImage*, *19* (2), Article 2. https://doi.org/10.1016/S1053-8119(03)00073-9

Dikecligil, G. N., & Gottfried, J. A. (2024). What Does the Human Olfactory System Do, and How Does It Do It? *Annual Review of Psychology*, *75* (1), null. https://doi.org/10.1146/annurev-psych-042023-101155

Donahue, M. J., Hoogduin, H., van Zijl, P. C. M., Jezzard, P., Luijten, P. R., & Hendrikse, J. (2011). Blood oxygenation level-dependent (BOLD) total and extravascular signal changes and ΔR2* in human visual cortex at 1.5, 3.0 and 7.0 T. *NMR in Biomedicine*, *24* (1), 25–34. https://doi.org/10.1002/nbm.1552

Donoshita, Y., Choi, U.-S., Ban, H., & Kida, I. (2021). Assessment of olfactory information in the human brain using 7-Tesla functional magnetic resonance imaging. *NeuroImage*, *236*, 118212. https://doi.org/10.1016/j.neuroimage.2021.118212

Dourado, G. B., Volpato, G. H., de Almeida-Pedrin, R. R., Pedron Oltramari, P. V., Freire Fernandes, T. M., & de Castro Ferreira Conti, A. C. (2021). Likert scale vs visual analog scale for assessing facial pleasantness. *American Journal of Orthodontics and Dentofacial Orthopedics*, *160* (6), 844–852. https://doi.org/10.1016/j.ajodo.2020.05.024

Dowdle, L. T., Vizioli, L., Moeller, S., Akçakaya, M., Olman, C., Ghose, G., Yacoub, E., & Uğurbil, K. (2023). Evaluating increases in sensitivity from NORDIC for diverse fMRI acquisition strategies. *NeuroImage*, *270*, 119949. https://doi.org/10.1016/j.neuroimage.2023.119949

DuPre, E., Salo, T., Ahmed, Z., Bandettini, P. A., Bottenhorn, K. L., Caballero-Gaudes, C., Dowdle, L. T., Gonzalez-Castillo, J., Heunis, S., Kundu, P., Laird, A. R., Markello, R., Markiewicz, C. J., Moia, S., Staden, I., Teves, J. B., Uruñuela, E., Vaziri-Pashkam, M., Whitaker, K., & Handwerker, D. A. (2021). TE-dependent analysis of multi-echo fMRI with *tedana*. *Journal of Open Source Software*, *6* (66), 3669. https://doi.org/10.21105/joss.03669

Esteban, O., Markiewicz, C. J., Blair, R. W., Moodie, C. A., Isik, A. I., Erramuzpe, A., Kent, J. D., Goncalves, M., DuPre, E., Snyder, M., Oya, H., Ghosh, S. S., Wright, J., Durnez, J., Poldrack, R. A., & Gorgolewski, K. J. (2019). fMRIPrep: A robust preprocessing pipeline for functional MRI. *Nature Methods*, *16* (1), Article 1. https://doi.org/10.1038/s41592-018-0235-4

Farinha, M., Amado, C., Morgado, P., & Cabral, J. (2022). Increased Excursions to Functional Networks in Schizophrenia in the Absence of Task. *Frontiers in Neuroscience*, *16*. https://www.frontiersin.org/articles/10.3389/fnins.2022.821179

Faul, F., Erdfelder, E., Buchner, A., & Lang, A.-G. (2009). Statistical power analyses using G*Power 3.1: Tests for correlation and regression analyses. *Behavior Research Methods*, *41* (4), 1149–1160. https://doi.org/10.3758/BRM.41.4.1149

Fera, F., Yongbi, M. N., van Gelderen, P., Frank, J. A., Mattay, V. S., & Duyn, J. H. (2004). EPI-BOLD fMRI of human motor cortex at 1.5 T and 3.0 T: Sensitivity dependence on echo time and acquisition bandwidth. *Journal of Magnetic Resonance Imaging*, *19* (1), 19–26. https://doi.org/10.1002/jmri.10440

Flint, A., Raben, A., Blundell, J. E., & Astrup, A. (2000). Reproducibility, power and validity of visual analogue scales in assessment of appetite sensations in single

test meal studies. *International Journal of Obesity*, *24* (1), Article 1. https://doi.org/10.1038/sj.ijo.0801083

Fonov, V., Evans, A. C., Botteron, K., Almli, C. R., McKinstry, R. C., & Collins, D. L. (2011). Unbiased average age-appropriate atlases for pediatric studies. *NeuroImage*, *54* (1), 313–327. https://doi.org/10.1016/j.neuroimage.2010.07.033

Fonov, V., Evans, A., McKinstry, R., Almli, C., & Collins, D. (2009). Unbiased nonlinear average age-appropriate brain templates from birth to adulthood. *NeuroImage*, *47*, S102. https://doi.org/10.1016/S1053-8119(09)70884-5

Fournel, A., Ferdenzi, C., Sezille, C., Rouby, C., & Bensafi, M. (2016). Multidimensional representation of odors in the human olfactory cortex. *Human Brain Mapping*, *37* (6), 2161–2172. https://doi.org/10.1002/hbm.23164

Friston, K. J., Glaser, D. E., Henson, R. N. A., Kiebel, S., Phillips, C., & Ashburner, J. (2002). Classical and Bayesian Inference in Neuroimaging: Applications. *NeuroImage*, *16* (2), 484–512. https://doi.org/10.1006/nimg.2002.1091

Gati, J. S., Menon, R. S., Uğurbil, K., & Rutt, B. K. (1997). Experimental determination of the BOLD field strength dependence in vessels and tissue. *Magnetic Resonance in Medicine*, *38* (2), 296–302. https://doi.org/10.1002/mrm.1910380220

Glover, G. H., & Law, C. S. (2001). Spiral-in/out BOLD fMRI for increased SNR and reduced susceptibility artifacts. *Magnetic Resonance in Medicine*, *46* (3), Article 3. https://doi.org/10.1002/mrm.1222

Gonzalez-Castillo, J., Panwar, P., Buchanan, L. C., Caballero-Gaudes, C., Handwerker, D. A., Jangraw, D. C., Zachariou, V., Inati, S., Roopchansingh, V., Derbyshire, J.

A., & Bandettini, P. A. (2016). Evaluation of multi-echo ICA denoising for task based fMRI studies: Block designs, rapid event-related designs, and cardiac-gated fMRI. *NeuroImage*, *141*, 452–468. https://doi.org/10.1016/j.neuroimage.2016.07.049

Gorgolewski, K., Burns, C., Madison, C., Clark, D., Halchenko, Y., Waskom, M., & Ghosh, S. (2011). Nipype: A Flexible, Lightweight and Extensible Neuroimaging Data Processing Framework in Python. *Frontiers in Neuroinformatics*, *5*. https://www.frontiersin.org/articles/10.3389/fninf.2011.00013

Gottfried, J. A., O'Doherty, J., & Dolan, R. J. (2003). Encoding Predictive Reward Value in Human Amygdala and Orbitofrontal Cortex. *Science*, *301* (5636), 1104–1107. https://doi.org/10.1126/science.1087919

Graham, S. J., Stanchev, P. L., & Bronskill, M. J. (1996). Criteria for analysis of multicomponent tissue T2 relaxation data. *Magnetic Resonance in Medicine*, *35* (3), 370–378. https://doi.org/10.1002/mrm.1910350315

Green, B. G., Dalton, P., Cowart, B., Shaffer, G., Rankin, K., & Higgins, J. (1996). Evaluating the 'Labeled Magnitude Scale' for Measuring Sensations of Taste and Smell. *Chemical Senses*, *21* (3), 323–334. https://doi.org/10.1093/chemse/21.3.323

Green, B. G., Shaffer, G. S., & Gilmore, M. M. (1993). Derivation and evaluation of a semantic scale of oral sensation magnitude with apparent ratio properties. *Chemical Senses*, *18* (6), 683–702. https://doi.org/10.1093/chemse/18.6.683

Howard, J. D., & Gottfried, J. A. (2014). Configural and Elemental Coding of Natural Odor Mixture Components in the Human Brain. *Neuron*, *84* (4), Article 4. https://doi.org/10.1016/j.neuron.2014.10.012

Howard, J. D., Plailly, J., Grueschow, M., Haynes, J.-D., & Gottfried, J. A. (2009). Odor quality coding and categorization in human posterior piriform cortex. *Nature Neuroscience*, *12* (7), Article 7. https://doi.org/10.1038/nn.2324

Im, K., Jo, H. J., Mangin, J.-F., Evans, A. C., Kim, S. I., & Lee, J.-M. (2010). Spatial Distribution of Deep Sulcal Landmarks and Hemispherical Asymmetry on the Cortical Surface. *Cerebral Cortex*, *20* (3), 602–611. https://doi.org/10.1093/cercor/bhp127

Jones, L. V., Peryam, D. R., & Thurstone, L. L. (1955). Development of a scale for measuring soldiers' food preferences. *Journal of Food Science*, *20* (5), 512–520. https://doi.org/10.1111/j.1365-2621.1955.tb16862.x

Jones, T. B., Bandettini, P. A., Kenworthy, L., Case, L. K., Milleville, S. C., Martin, A., & Birn, R. M. (2010). Sources of group differences in functional connectivity: An investigation applied to autism spectrum disorder. *NeuroImage*, *49* (1), 401–414. https://doi.org/10.1016/j.neuroimage.2009.07.051

Kelly, R. E., Alexopoulos, G. S., Wang, Z., Gunning, F. M., Murphy, C. F., Morimoto, S. S., Kanellopoulos, D., Jia, Z., Lim, K. O., & Hoptman, M. J. (2010). Visual inspection of independent components: Defining a procedure for artifact removal from fMRI data. *Journal of Neuroscience Methods*, *189* (2), 233–245. https://doi.org/10.1016/j.jneumeth.2010.03.028

Kundu, P., Brenowitz, N. D., Voon, V., Worbe, Y., Vértes, P. E., Inati, S. J., Saad, Z. S., Bandettini, P. A., & Bullmore, E. T. (2013). Integrated strategy for improving functional connectivity mapping using multiecho fMRI. *Proceedings of the National Academy of Sciences*, *110* (40), 16187–16192. https://doi.org/10.1073/pnas.1301725110

Kundu, P., Inati, S. J., Evans, J. W., Luh, W.-M., & Bandettini, P. A. (2012a). Differentiating BOLD and non-BOLD signals in fMRI time series using multi-echo EPI. *NeuroImage*, *60* (3), 1759–1770. https://doi.org/10.1016/j.neuroimage.2011.12.028

Kundu, P., Inati, S. J., Evans, J. W., Luh, W.-M., & Bandettini, P. A. (2012b). Differentiating BOLD and non-BOLD signals in fMRI time series using multi-echo EPI. *NeuroImage*, *60* (3), 1759–1770. https://doi.org/10.1016/j.neuroimage.2011.12.028

Kundu, P., Voon, V., Balchandani, P., Lombardo, M. V., Poser, B. A., & Bandettini, P. A. (2017). Multi-echo fMRI: A review of applications in fMRI denoising and analysis of BOLD signals. *NeuroImage*, *154*, 59–80. https://doi.org/10.1016/j.neuroimage.2017.03.033

Levene, H. (1960). Robust tests for equality of variances. *Contributions to Probability and Statistics*, 278–292.

Lim, J., Wood, A., & Green, B. G. (2009). Derivation and Evaluation of a Labeled Hedonic Scale. *Chemical Senses*, *34* (9), 739–751. https://doi.org/10.1093/chemse/bjp054

Lynch, C. J., Power, J. D., Scult, M. A., Dubin, M., Gunning, F. M., & Liston, C. (2020). Rapid Precision Functional Mapping of Individuals Using Multi-Echo fMRI. *Cell Reports*, *33* (12), 108540. https://doi.org/10.1016/j.celrep.2020.108540

Mai, J. K., Majtanik, M., & Paxinos, G. (2016). *Atlas of the human brain* (4th edition). Academic Press.

Manera, A. L., Dadar, M., Fonov, V., & Collins, D. L. (2020). CerebrA, registration and manual label correction of Mindboggle-101 atlas for MNI-ICBM152 template. *Scientific Data*, *7* (1), Article 1. https://doi.org/10.1038/s41597-020-0557-9

McKeown, M. J., Hansen, L. K., & Sejnowsk, T. J. (2003). Independent component analysis of functional MRI: What is signal and what is noise? *Current Opinion in Neurobiology*, *13* (5), 620–629. https://doi.org/10.1016/j.conb.2003.09.012

Mckeown, M. J., Makeig, S., Brown, G. G., Jung, T.-P., Kindermann, S. S., Bell, A. J., & Sejnowski, T. J. (1998). Analysis of fMRI data by blind separation into independent spatial components. *Human Brain Mapping*, *6* (3), 160–188. https://doi.org/10.1002/(SICI)1097-0193(1998)6:3<160::AID-HBM5>3.0.CO;2-1

Miao, X., Paez, A. G., Rajan, S., Cao, D., Liu, D., Pantelyat, A. Y., Rosenthal, L. I., van Zijl, P. C. M., Bassett, S. S., Yousem, D. M., Kamath, V., & Hua, J. (2021). Functional Activities Detected in the Olfactory Bulb and Associated Olfactory Regions in the Human Brain Using T2-Prepared BOLD Functional MRI at 7T. *Frontiers in Neuroscience*, *15*. https://www.frontiersin.org/articles/10.3389/fnins.2021.723441

Moeller, S., Pisharady, P. K., Ramanna, S., Lenglet, C., Wu, X., Dowdle, L., Yacoub, E., Uğurbil, K., & Akçakaya, M. (2021). NOise reduction with DIstribution Corrected

(NORDIC) PCA in dMRI with complex-valued parameter-free locally low-rank processing. *NeuroImage*, *226*, 117539. https://doi.org/10.1016/j.neuroimage.2020.117539

Parrish, T., Chen, Y., Li, W., Howard, J., & Gottfried, J. (2008). High resolution 3D functional images of the human olfactory bulb using passband SSFP at 3T. *Proceedings of International Society of Magnetic Resonance in Medicine*, 3567.

Patin, A., & Pause, B. M. (2015). Human amygdala activations during nasal chemoreception. *Neuropsychologia*, *78*, 171–194. https://doi.org/10.1016/j.neuropsychologia.2015.10.009

Perszyk, E. E., Davis, X. S., & Small, D. M. (2023). Olfactory decoding is positively associated with ad libitum food intake in sated humans. *Appetite*, *180*, 106351. https://doi.org/10.1016/j.appet.2022.106351

Plailly, J., Howard, J. D., Gitelman, D. R., & Gottfried, J. A. (2008). Attention to Odor Modulates Thalamocortical Connectivity in the Human Brain. *Journal of Neuroscience*, *28* (20), 5257–5267. https://doi.org/10.1523/JNEUROSCI.5607-07.2008

Poser, B. A., Versluis, M. J., Hoogduin, J. M., & Norris, D. G. (2006). BOLD contrast sensitivity enhancement and artifact reduction with multiecho EPI: Parallel-acquired inhomogeneity-desensitized fMRI. *Magnetic Resonance in Medicine*, *55* (6), 1227–1235. https://doi.org/10.1002/mrm.20900

Posse, S., Wiese, S., Gembris, D., Mathiak, K., Kessler, C., Grosse-Ruyken, M.-L., Elghahwagi, B., Richards, T., Dager, S. R., & Kiselev, V. G. (1999). Enhancement of BOLD-contrast sensitivity by single-shot multi-echo functional

MR imaging. *Magnetic Resonance in Medicine*, *42* (1), 87–97. https://doi.org/10.1002/(SICI)1522-2594(199907)42:1<87::AID-MRM13>3.0.CO;2-O

Raithel, C. U., Miller, A. J., Epstein, R. A., Kahnt, T., & Gottfried, J. A. (2023). Recruitment of grid-like responses in human entorhinal and piriform cortices by odor landmark-based navigation. *Current Biology*, *33* (17), 3561-3570.e4. https://doi.org/10.1016/j.cub.2023.06.087

Raj, D., Anderson, A. W., & Gore, J. C. (2001). Respiratory effects in human functional magnetic resonance imaging due to bulk susceptibility changes. *Physics in Medicine & Biology*, *46* (12), 3331. https://doi.org/10.1088/0031-9155/46/12/318

Raj, D., Paley, D. P., Anderson, A. W., Kennan, R. P., & Gore, J. C. (2000). A model for susceptibility artefacts from respiration in functional echo-planar magnetic resonance imaging. *Physics in Medicine & Biology*, *45* (12), 3809. https://doi.org/10.1088/0031-9155/45/12/321

Roth, Z. N., Ryoo, M., & Merriam, E. P. (2020). Task-related activity in human visual cortex. *PLOS Biology*, *18* (11), e3000921. https://doi.org/10.1371/journal.pbio.3000921

Savic, I. (2002). Imaging of brain activation by odorants in humans. *Current Opinion in Neurobiology*, *12* (4), 455–461. https://doi.org/10.1016/S0959-4388(02)00346-X

Savic, I., Gulyás, B., & Berglund, H. (2002). Odorant differentiated pattern of cerebral activation: Comparison of acetone and vanillin. *Human Brain Mapping*, *17* (1), 17–27. https://doi.org/10.1002/hbm.10045

Schutz, H. G., & Cardello, A. V. (2001). A Labeled Affective Magnitude (lam) Scale for Assessing Food Liking/Disliking1. *Journal of Sensory Studies*, *16* (2), 117–159. https://doi.org/10.1111/j.1745-459X.2001.tb00293.x

Shanahan, L. K., Bhutani, S., & Kahnt, T. (2021). Olfactory perceptual decision-making is biased by motivational state. *PLOS Biology*, *19* (8), e3001374. https://doi.org/10.1371/journal.pbio.3001374

Stone, H., Bleibaum, R. N., & Thomas, H. A. (2020). *Sensory evaluation practices*. Academic press.

Swarup, S., Huang, W., Mackay, T. F. C., & Anholt, R. R. H. (2013). Analysis of natural variation reveals neurogenetic networks for Drosophila olfactory behavior. *Proceedings of the National Academy of Sciences*, *110* (3), 1017–1022. https://doi.org/10.1073/pnas.1220168110

Triantafyllou, C., Wald, L. L., & Hoge, R. D. (2011). Echo-Time and Field Strength Dependence of BOLD Reactivity in Veins and Parenchyma Using Flow-Normalized Hypercapnic Manipulation. *PLOS ONE*, *6* (9), e24519. https://doi.org/10.1371/journal.pone.0024519

Van, A. N., Tisdall, M. D., Laumann, T. O., Montez, D. F., Fair, D. A., & Dosenbach, N. U. F. (2023). Framewise distortion correction in Multi-echo Echo Planar Imaging. *Proceedings of International Society of Magnetic Resonance in Medicine*.

Van de Moortele, P.-F., Pfeuffer, J., Glover, G. H., Ugurbil, K., & Hu, X. (2002). Respiration-induced B0 fluctuations and their spatial distribution in the human brain at 7 Tesla. *Magnetic Resonance in Medicine*, *47* (5), 888–895. https://doi.org/10.1002/mrm.10145

van der Zwaag, W., Francis, S., Head, K., Peters, A., Gowland, P., Morris, P., & Bowtell, R. (2009). fMRI at 1.5, 3 and 7 T: Characterising BOLD signal changes. *NeuroImage*, *47* (4), 1425–1434. https://doi.org/10.1016/j.neuroimage.2009.05.015

Vizioli, L., Moeller, S., Dowdle, L., Akçakaya, M., De Martino, F., Yacoub, E., & Uğurbil, K. (2021). Lowering the thermal noise barrier in functional brain mapping with magnetic resonance imaging. *Nature Communications*, *12* (1), Article 1. https://doi.org/10.1038/s41467-021-25431-8

Weiskopf, N., Hutton, C., Josephs, O., & Deichmann, R. (2006). Optimal EPI parameters for reduction of susceptibility-induced BOLD sensitivity losses: A whole-brain analysis at 3 T and 1.5 T. *NeuroImage*, *33* (2), 493–504. https://doi.org/10.1016/j.neuroimage.2006.07.029

Yekutieli, D., & Benjamini, Y. (1999). Resampling-based false discovery rate controlling multiple test procedures for correlated test statistics. *Journal of Statistical Planning and Inference*, *82* (1), 171–196. https://doi.org/10.1016/S0378-3758(99)00041-5

Zhou, G., Lane, G., Cooper, S. L., Kahnt, T., & Zelano, C. (2019). Characterizing functional pathways of the human olfactory system. *eLife*, *8*, e47177. https://doi.org/10.7554/eLife.47177